Contribution from the Department of Chemistry and Materials Research Center, Northwestern University, Evanston, Illinois 60208

Structural and Charge Transport Properties of Bis[(5,10,15,20-tetramethylporphyrinato)nickel(II)] Perrhenate, $[Ni(tmp)]_2[ReO_4]$

Timothy P. Newcomb, Martin R. Godfrey, Brian M. Hoffman,* and James A. Ibers*

Received June 19, 1989

Electrochemical oxidation of (5,10,15,20-tetramethylporphyrinato)nickel(II), Ni(tmp), in the presence of the perrhenate ion affords the new molecular conductor $[Ni(tmp)]_2[ReO_4]$, which is composed of planar Ni(tmp) molecules stacked metal-over-metal. The two unique Ni(tmp) molecules within the cell are on sites of 4 symmetry, are separated by 3.355 (2) Å, and are rotated with respect to one another by 27.5 (1)° about the *c* axis (stacking direction). The ReO_4^- anion lies on a site of $\bar{4}$ symmetry within a channel formed by adjacent porphyrin stacks. ESR measurements confirm the tmp ligand as the site of oxidation. Single-crystal room-temperature conductivity along the needle (crystallographic *c*) axis averages 90 Ω^{-1} cm^{-1}, typical for tmp-based conductors. The temperature dependence of the conductivity is thermally activated and has been fit to an expression describing a semiconductor with temperature-dependent carrier mobility; $\sigma = \sigma_0 T^{-\alpha} \exp(-E_g/kT)$ (E_g = 0.24 (2) eV, $3.5 < \alpha < 18$). Previously synthesized Ni(tmp)-based conductors exhibit metal-like conductivities at high temperatures. The semiconducting nature of the conductivity in the present compound is attributed to a small transfer integral between the π molecular orbitals on adjacent intrastack porphyrin rings as a consequence of the 27.5° rotation angle between independent rings. The compound crystallizes in space group C_{4h}^3-$P4/n$ of the tetragonal system with two formula units in a cell of dimensions a = 16.710 (4) Å and c = 6.720 (2) Å (V = 1876 Å^3) at 125 K. Full-matrix least-squares refinement of 144 variables gives a final value of 0.085 for the R index on F^2 for 2742 unique observations and a value of 0.052 for the R index on F for the 1850 observations having $F_o^2 > 3\sigma(F_o^2)$.

Introduction

During the past 10 years a series of partially oxidized molecular conductors have been prepared by chemical oxidation of porphyrinic metallomacrocycles (M(L)) with molecular iodine[1-8] or by electrochemical oxidation of the same porphyrins in the presence of a suitable electrolyte.[9-11] A single structural motif has been retained throughout this series of materials, with metal-over-metal stacks of partially oxidized M(L) units surrounded by chains of anions. The arrangement of the rings within a stack can be described as an ABAB pattern, and with one exception,[7,12] the rotation angle, ϕ, between macrocycle A and macrocycle B is ~40°. This arrangement is depicted in Figure 1. In the conductors composed of benzoporphyrins (pc, tatbp, tbp),[14] all the stacks are identical with each other. In the tmp systems reported to date,[1,11] each stack is shifted from adjacent stacks by $z = {}^1/_2$.

We have previously discussed the relationship between anion size and metallomacrocycle stacking structure in porphyrinic conductors.[11] We now report the structural, magnetic, and charge-transport properties of the molecular conductor bis[(5,10,15,20-tetramethylporphyrinato)nickel(II)] perrhenate, $[Ni(tmp)]_2[ReO_4]$, a system in which the Ni(tmp) stacking structure has changed in several significant ways from previously prepared Ni(tmp) conductors, presumably to accommodate the large perrhenate anion. As in all other metallomacrocyclic conductors, $[Ni(tmp)]_2[ReO_4]$ possesses metal-over-metal stacks in which adjacent macrocycles are staggered by an angle, ϕ. For $[Ni(tmp)]_2[ReO_4]$, ϕ = 27.5 (1)°, one of the smallest rotation angles observed to date in this class of conductors. This reduced value of ϕ is attributed to close porphyrin–hydrogen anion–oxygen contacts and has dramatic consequences for the physical properties of this material.

Table I. Crystal Data and Experimental Details for $[Ni(tmp)]_2[ReO_4]$

compd	bis[(5,10,15,20-tetramethylporphyrinato)-nickel(II)] perrhenate
formula	$C_{48}H_{40}N_8Ni_2O_4Re$
fw	1096.52
cell consts	
a, Å	16.710 (4)
c, Å	6.720 (2)
V, Å^3	1876
Z	2
temp, K	125
d_{calc}, g/cm^3	1.940
space group	C_4^3-$P4/n$
radiation	Mo Kα (λ(Mo Kα) = 0.7093 Å); graphite-monochromated
μ, cm^{-1}	43.2
transm factors	0.59–0.64
R on F_o^2	0.085
R_w on F_o^2	0.120
R on F_o, $F_o^2 > 3\sigma(F_o^2)$	0.052
R_w on F_o, $F_o^2 > 3\sigma(F_o^2)$	0.059

Experimental Section

Preparation of $[Ni(tmp)]_2[ReO_4]$. Ni(tmp) was prepared as described previously.[15] Single crystals of $[Ni(tmp)]_2[ReO_4]$ were grown at the anode of an electrolytic cell that consisted of two compartments separated by a frit of medium porosity. The anode compartment was filled with a 1,1,2-trichloroethane solution that was 10^{-3} M in Ni(tmp) and 10^{-2} M in $[N(n\text{-}Bu)_4][ReO_4]$. The cathode compartment was filled with a 1,1,2-trichloroethane solution that was 10^{-2} M in $[N(n\text{-}Bu)_4][ReO_4]$. Platinum electrodes were immersed in both compartments, and a constant current of 2.0 μA was passed through the cell for 1 week. Needle-shaped crystals of $[Ni(tmp)]_2[ReO_4]$, octagonal in cross section, were harvested

(1) Pace, L. J.; Martinsen, J.; Ulman, A.; Hoffman, B. M.; Ibers, J. A. *J. Am. Chem. Soc.* **1983**, *105*, 2612-2620.
(2) Ogawa, M. Y.; Hoffman, B. M.; Lee, S.; Yadkowsky, M.; Halperin, W. P. *Phys. Rev. Lett.* **1986**, *57*, 1177-1180.
(3) Martinsen, J.; Stanton, J. L.; Greene, R. L.; Tanaka, J.; Hoffman, B. M.; Ibers, J. A. *J. Am. Chem. Soc.* **1985**, *107*, 6915-6920.
(4) Hoffman, B. M.; Ibers, J. A. *Acc. Chem. Res.* **1983**, *16*, 15-21.
(5) Martinsen, J.; Pace, L. J.; Phillips, T. E.; Hoffman, B. M.; Ibers, J. A. *J. Am. Chem. Soc.* **1982**, *104*, 83-91.
(6) Schramm, C. J.; Scaringe, R. P.; Stojakovic, D. R.; Hoffman, B. M.; Ibers, J. A.; Marks, T. J. *J. Am. Chem. Soc.* **1980**, *102*, 6702-6713.
(7) Phillips, T. E.; Scaringe, R. P.; Hoffman, B. M.; Ibers, J. A. *J. Am. Chem. Soc.* **1980**, *102*, 3435-3444.
(8) Wright, S. K.; Schramm, C. J.; Phillips, T. E.; Scholler, D. M.; Hoffman, B. M. *Synth. Met.* **1979**, *1*, 43-51.
(9) Yakushi, K.; Sakuda, M.; Hamada, I.; Kuroda, H.; Kawamoto, A.; Tanaka, J.; Sugano, T.; Kinoshita, M. *Synth. Met.* **1987**, *19*, 769-774.
(10) Almeida, M.; Kanatzidis, M. G.; Tonge, L. M.; Marks, T. J.; Marcy, H. O.; McCarthy, W. J.; Kannewurf, C. R. *Solid State Commun.* **1987**, *63*, 457-461.
(11) Newcomb, T. P.; Godfrey, M. R.; Hoffman, B. M.; Ibers, J. A. *J. Am. Chem. Soc.* **1989**, *111*, 7078-7084.
(12) The two metallamacrocycles in the unit cell of Ni(omtbp)I are rotated by 26° with respect to each other. However, the intrastack separation is 3.78 Å, well beyond the van der Waals contact distance (see ref 13).
(13) Bondi, A. *J. Phys. Chem.* **1964**, *68*, 441-451.
(14) Abbreviations used: tmp, 5,10,15,20-tetramethylporphyrinato; tbp, tetrabenzoporphyrinato; tatbp, triazatetrabenzoporphyrinato; omtbp, 1,4,5,8,9,12,13,16-octamethyltetrabenzoporphyrinato; pc, phthalocyaninato; oep, 2,3,7,8,12,13,17,18-octaethylporphyrinato; *n*-Bu, *n*-butyl.
(15) (a) Ulman, A.; Gallucci, J.; Fisher, D.; Ibers, J. A. *J. Am. Chem. Soc.* **1980**, *102*, 6852-6854. (b) Ulman, A.; Fisher, D.; Ibers, J. A. *J. Heterocycl. Chem.* **1982**, *19*, 409-413.

0020-1669/90/1329-0223$02.50/0

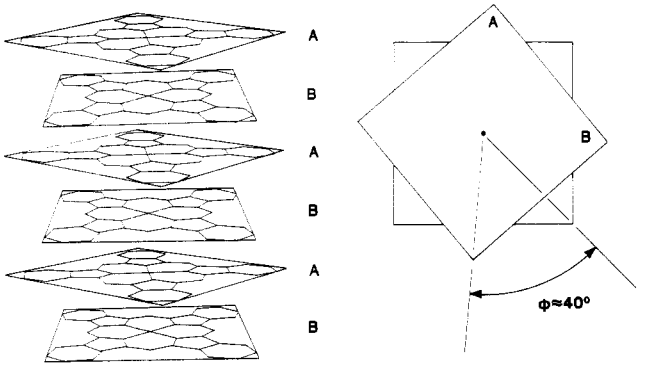

Figure 1. Usual stacking pattern of metalloporphyrin units in porphyrin-based conductors. ϕ is the rotation angle between the two units.

from the anode surface. Semiquantitative analysis performed with the use of an EDAX-equipped scanning electron microscope determined the Ni/Re ratio to be approximately 2/1. Trace amounts of chlorine were detected but were not judged to be significant.

Single-Crystal Electrical Conductivity Measurements. The electrical conductivity along the needle (c) axis of single crystals of $[Ni(tmp)]_2[ReO_4]$ was measured with a four-probe ac (27 Hz) phase-locked technique as described previously.[16] The temperature was controlled with a nitrogen gas flow Dewar assembly. The temperature was monitored to a precision of ±1.0 K with a copper–constantan thermocouple located within the sample holder. The rate of cooling varied between 0.5–0.1 deg/min. The uncertainties in the measurements of sample dimensions, which varied within the ranges of 0.3–0.8 mm in length and 4×10^{-4}–1.0×10^{-3} mm^2 in cross-sectional area, are estimated to cause an uncertainty in the absolute conductivity of $\Delta(\sigma)/\sigma = \pm 0.2$. These needle-shaped crystals are too thin to enable the measurement of conductivity perpendicular to the needle axis.

X-ray Diffraction Study of $[Ni(tmp)]_2[ReO_4]$. From Weissenberg photographs, crystals of $[Ni(tmp)]_2[ReO_4]$ were assigned to Laue group $4/m$ of the tetragonal system. The systematic absences ($hk0$, $h + k$ odd; $00l$, hhl, l odd) are consistent with space group C_{4h}^3-$P4/n$. The cell constants of a = 16.710 (4) Å and c = 6.720 (2) Å at 125 K were determined by a least-squares refinement of the setting angles of 16 reflections that had been hand-centered on a FACS-I diffractometer. Intensity data were collected at 125 K by the θ–2θ technique and processed by methods standard in this laboratory.[17] A total of 2950 reflections were collected, of which 2742 are unique and 1850 have $F_o^2 > 3\sigma(F_o^2)$. Crystal data and experimental details are summarized in Table I; more information is available in Table IS.[18]

A Patterson map indicated that the position of the rhenium atom is displaced by 0, $^1/_2$, 0.1 and 0, $^1/_2$, 0.4 from the nickel atom positions. The orientation of the porphyrin rings was determined by an examination of the rhenium-to-porphyrin atom vectors. The expected tetrahedral symmetry of the ReO_4^- anion, the observation of the rhenium–rhenium vector at $^1/_2$, $^1/_2$, 0, and the presence of two formula units per cell limit the choice for rhenium atom positions in space group $P4/n$ (unit cell origin at $\bar{1}$) to sites 2a or 2b, both with $\bar{4}$ symmetry. We placed the rhenium atom in site 2b (symmetry $\bar{4}$), thus constraining the two independent nickel atoms to the 2c sites of symmetry 4.

Initial refinements were carried out on F_o with the 1859 unique reflections having $F_o^2 > 3\sigma(F_o^2)$. All non-hydrogen atom positions were determined from subsequent electron density maps. After we had established the composition of the material, we corrected the data for absorption. Least-squares refinement on F_o with isotropic thermal parameters of all non-hydrogen atoms led to values of R and R_w of 0.18 and 0.20, respectively. When anisotropic thermal parameters were used, R and R_w decreased to 0.091 and 0.105, respectively. All hydrogen atom positions were located on a difference electron density map, and these were idealized (C–H = 0.95 Å) and not varied. Each hydrogen atom was assigned an isotropic thermal parameter 1 Å^2 greater than the equivalent isotropic thermal parameter of the carbon atom to which it is bonded. The final refinement was carried out on F_o^2 and involved 144 variables and all 2742 unique data (including $F_o^2 < 0$). This refinement converged to the agreement indices given in Table I. Final positional and equivalent isotropic thermal parameters are given in Table II. Additional crystallographic details are given in the supplementary material.[18]

Table II. Positional Parameters and Equivalent Isotropic Thermal Parameters for $[Ni(tmp)]_2[ReO_4]$

atom	x	y	z	B, Å^2
Ni(1)	$^1/_4$	$^1/_4$	0.37498 (16)	0.81 (1)
Ni(2)	$-^1/_4$	$-^1/_4$	0.12423 (16)	0.83 (1)
Re	$^1/_4$	$^3/_4$	$^1/_2$	2.336 (8)
N(1)	0.14498 (17)	0.19761 (17)	0.37575 (53)	0.86 (6)
C(11)	0.12880 (21)	0.11615 (21)	0.37398 (63)	1.05 (7)
C(12)	0.04379 (21)	0.10310 (22)	0.37234 (70)	1.26 (8)
C(13)	0.00813 (21)	0.17492 (21)	0.37358 (71)	1.27 (8)
C(14)	0.07149 (20)	0.23370 (21)	0.37503 (64)	0.96 (7)
C(15)	0.18454 (22)	0.05573 (21)	0.37389 (67)	1.15 (8)
C(16)	0.15818 (22)	−0.03108 (21)	0.37295 (77)	1.50 (8)
N(2)	−0.18087 (17)	−0.15551 (17)	0.12448 (54)	0.98 (6)
C(21)	−0.20301 (22)	−0.07641 (20)	0.12662 (66)	1.11 (8)
C(22)	−0.13390 (24)	−0.02485 (22)	0.12733 (70)	1.46 (8)
C(23)	−0.06892 (23)	−0.07221 (23)	0.12404 (72)	1.55 (9)
C(24)	−0.09735 (20)	−0.15383 (22)	0.12380 (67)	1.13 (8)
C(25)	−0.04699 (21)	−0.21922 (22)	0.12441 (69)	1.21 (8)
C(26)	0.04246 (22)	−0.20529 (23)	0.12252 (78)	1.60 (9)
O	0.30314 (18)	−0.18401 (17)	0.35219 (66)	2.8 (1)
H1C(12)	0.018	0.051	0.371	2.2
H1C(13)	−0.049	0.186	0.374	2.3
H1C(22)	−0.134	0.033	0.130	2.4
H1C(23)	−0.014	−0.055	0.121	2.5
H1C(16)	0.152	−0.050	0.506	2.5
H2C(16)	0.109	−0.037	0.304	2.5
H3C(16)	0.198	−0.063	0.308	2.5
H1C(26)	0.062	−0.203	0.256	2.5
H2C(26)	0.069	−0.248	0.054	2.5
H3C(26)	0.055	−0.156	0.058	2.5

Electron Spin Resonance Measurements. Powder and single-crystal electron spin resonance spectra were obtained on a modified Varian E-4 X-band spectrometer with 100-kHz field modulation as described previously.[7] A single crystal of $[Ni(tmp)]_2[ReO_4]$ was mounted on a quartz rod that was attached to a goniometer and placed in the resonance cavity of the spectrometer. The crystal was oriented such that the needle (c) axis could be positioned parallel or perpendicular to the applied field and rotated through intermediate angles. Rotation angles were measured to a precision of ±1.0°. Spin susceptibility measurements were made with powdered samples of $[Ni(tmp)]_2[ReO_4]$ at room temperature and 77 K. A sample of Ni(pc)I was used as the spin susceptibility standard, since it has an accurately known spin susceptibility value and its ESR properties are similar to those of $[Ni(tmp)]_2[ReO_4]$.[6]

Magnetic Susceptibility Measurements. Static magnetic susceptibility measurements were taken with an SHE VTS-50 SQUID susceptometer. The sample holder was made of high-purity Spectrosil quartz (Thermal American, Inc.), and its background magnetic contribution was measured over the full temperature range prior to measurements on the sample. The sample magnetism was determined at a field strength of 5 kG from the average of ten measurements made at each temperature. The sample weight was 18.4 mg. The room-temperature magnetization was determined with a 22-mg sample at 10 kG after calibration of the instrument.

Results and Discussion

Description of the Structure. The unit cell constants of $[Ni(tmp)]_2[ReO_4]$ are similar to those of Ni(tmp)I[1] and $[Ni(tmp)]_2[PF_6]$.[11] Unlike these compounds, however, the $[Ni(tmp)]_2[ReO_4]$ unit cell contains two unique Ni(tmp) rings, rather than one. The arrangement of these rings is similar. As for other tmp conductors, $[Ni(tmp)]_2[ReO_4]$ is composed of columns of Ni(tmp) cations surrounded by anions. Figure 2 shows the stacking of Ni(tmp) groups viewed along the [001] direction. These groups have crystallographically imposed 4 symmetry, and they stack metal-over-metal with their mean planes orthogonal to the c axis. The Ni–Ni spacings along a stack alternate, with the Ni(1)–Ni(2) and Ni(2)–Ni′(1) distances being 3.355 (2) and 3.365 (2) Å, respectively. This alternation is not statistically significant, and thus we still often refer to a regular stack with an averaged Ni–Ni spacing. The anion lies on a site of crystallographically imposed $\bar{4}$ symmetry within the channels formed by the Ni(tmp) columns. The arrangement of the anions with respect to the columns and the columns with respect to each other in $[Ni(tmp)]_2[ReO_4]$ is unique among the tmp conductors; the anions are at the same level in the unit cell along the c axis, and

(16) Phillips, T. E.; Anderson, J. R.; Schramm, C. J.; Hoffman, B. M. *Rev. Sci. Instrum.* **1979**, *50*, 263–265.
(17) Corfield, P. W. R.; Doedens, R. J.; Ibers, J. A. *Inorg. Chem.* **1967**, *6*, 197–204.
(18) See paragraph at end of paper regarding supplementary material.

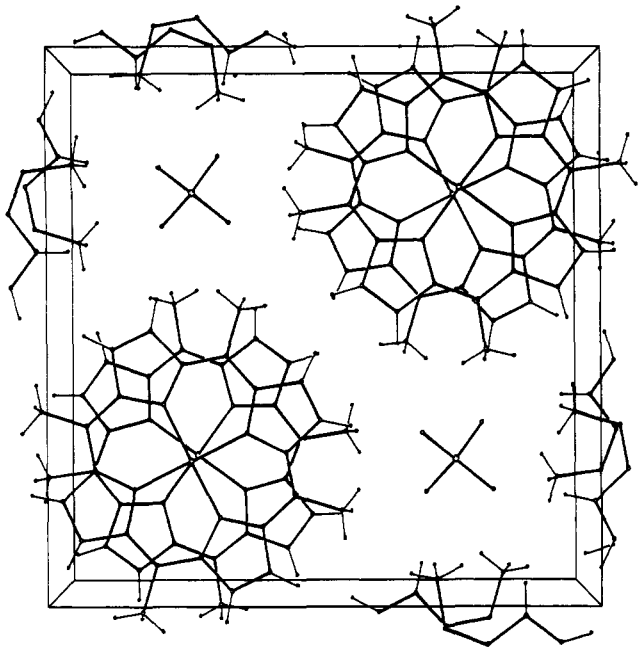

Figure 2. Structure of [Ni(tmp)]$_2$[ReO$_4$], as viewed along the [001] direction.

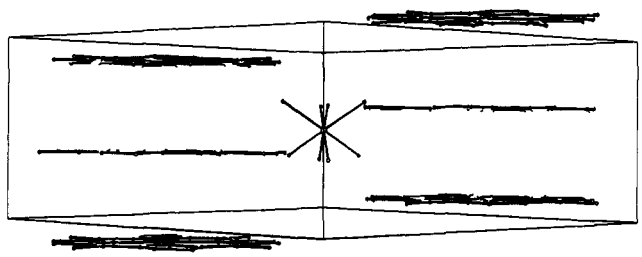

Figure 3. Structure of [Ni(tmp)]$_2$[ReO$_4$], as viewed along the [110] direction.

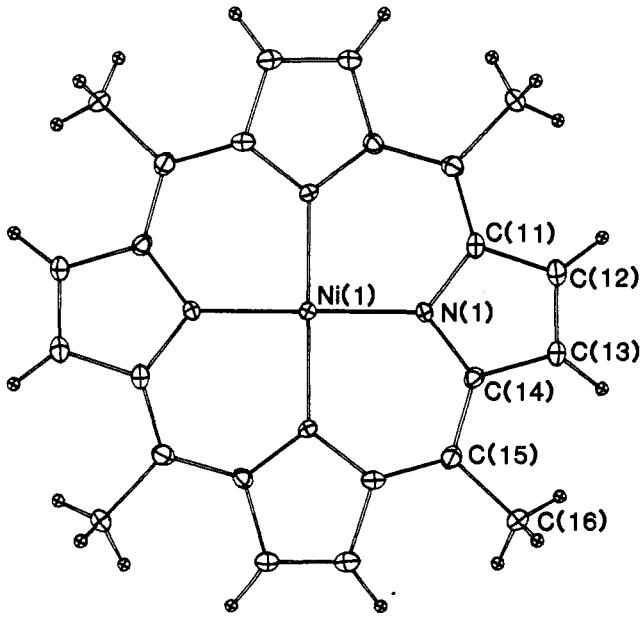

Figure 4. Drawing of one Ni(tmp) molecule with its labeling scheme. Thermal ellipsoids are drawn at the 50% level except for H atoms, which are drawn arbitrarily small.

adjacent average stacks of Ni(tmp) molecules are shifted by essentially $c/4$ with respect to one another. This relationship is depicted in Figure 3.

The Ni(tmp) Cation. There are two independent Ni(tmp) cations in the crystal structure of [Ni(tmp)]$_2$[ReO$_4$]. A drawing of one cation with its labeling scheme is shown in Figure 4. Table III summarizes the intramolecular bond distances and angles for [Ni(tmp)]$_2$[ReO$_4$]. Comparison of these structural features demonstrates that, although they are crystallographically distinct, the two rings are chemically equivalent. The Ni(tmp) cations (symmetry 4) are planar (maximum deviation 0.014 Å), though this is not a crystallographically imposed condition. The best

Table III. Distances and Angles for [Ni(tmp)]$_2$[ReO$_4$]

bond	type[a]	dist, Å	av[b]
Ni(1)–Ni(2)		3.355 (2)	3.360 (3)
Ni(2)–Ni′(1)		3.365 (2)	
Ni(1)–N(1)	M–N	1.961 (4)	1.959 (4)
Ni(2)–N(2)		1.956 (4)	
N(1)–C(11)	N–C$_a$	1.388 (6)	1.381 (13)
N(1)–C(14)		1.368 (5)	
N(2)–C(21)		1.373 (6)	
N(2)–C(24)		1.396 (6)	
C(11)–C(12)	C$_a$–C$_b$	1.437 (6)	1.442 (6)
C(13)–C(14)		1.444 (6)	
C(21)–C(22)		1.441 (7)	
C(23)–C(24)		1.444 (6)	
C(12)–C(13)	C$_b$–C$_b$	1.340 (7)	1.342 (7)
C(22)–C(23)		1.344 (7)	
C(11)–C(15)	C$_a$–C$_m$	1.374 (6)	1.384 (9)
C(14)–C(15)		1.392 (6)	
C(21)–C(25)		1.390 (6)	
C(24)–C(25)		1.379 (6)	
C(15)–C(16)	C$_m$–C$_t$	1.516 (6)	1.515 (7)
C(25)–C(26)		1.513 (7)	
Re–O		1.729 (4)	

bond	type[a]	angle, deg	av[b]
N(1)–Ni(1)–N(1)	N–M–N′	90	90
N(2)–Ni(2)–N(2)		90	
Ni(1)–N(1)–C(11)	M–N–C$_a$	127.7 (3)	127.6 (4)
Ni(1)–N(1)–C(14)		127.3 (3)	
Ni(2)–N(2)–C(21)		128.2 (3)	
Ni(2)–N(2)–C(24)		127.3 (3)	
C(11)–N(1)–C(14)	C$_a$–N–C$_a$	104.9 (4)	104.7 (4)
C(22)–N(2)–C(24)		104.5 (4)	
N(1)–C(11)–C(12)	N–C$_a$–C$_b$	110.0 (4)	110.6 (5)
N(1)–C(14)–C(13)		111.0 (4)	
N(2)–C(21)–C(22)		111.1 (4)	
N(2)–C(24)–C(23)		110.4 (4)	
N(1)–C(11)–C(15)	N–C$_a$–C$_m$	126.1 (4)	126.5 (4)
N(1)–C(14)–C(15)		127.1 (4)	
N(2)–C(21)–C(25)		126.3 (4)	
N(2)–C(24)–C(25)		126.4 (4)	
C(11)–C(12)–C(13)	C$_a$–C$_b$–C$_b$	107.7 (4)	107.1 (5)
C(12)–C(13)–C(14)		106.4 (4)	
C(21)–C(22)–C(23)		107.2 (4)	
C(22)–C(23)–C(24)		106.9 (4)	
C(12)–C(11)–C(15)	C$_b$–C$_a$–C$_m$	124.0 (4)	122.9 (9)
C(13)–C(14)–C(15)		121.9 (4)	
C(22)–C(21)–C(25)		122.6 (4)	
C(23)–C(24)–C(25)		123.2 (4)	
C(11)–C(15)–C(14)	C$_a$–C$_m$–C$_a$	121.8 (4)	121.8 (4)
C(21)–C(25)–C(24)		121.7 (4)	
C(11)–C(15)–C(16)	C$_a$–C$_7$–C$_t$	120.4 (4)	119 (1)
C(14)–C(15)–C(16)		117.8 (4)	
C(21)–C(25)–C(26)		119.6 (4)	
C(24)–C(25)–C(26)		118.8 (4)	
O–Re–O		109.3 (2)	
		109.9 (3)	

rotation angle between intrastack Ni(tmp) molecules: 27.5 (1)°

[a] The notation is that of Hoard (Hoard, J. L. *Science* (*Washington D.C.*) **1971**, *174*, 1295–1302); C_t is the methyl group on the methine carbon. [b] The number of parentheses is the larger of the standard deviation of a single observation as estimated from the inverse matrix or from the values averaged.

Table IV. Least-Squares Planes in $[Ni(tmp)]_2[ReO_4]$

	dev from plane, Å			
	ring n = 1		ring n = 2	
atoms	plane 1 z = 0.3744[a]	plane 2 pyrrole	plane 1′ z = 0.125[a]	plane 2′ pyrrole
Ni(n)	0.004		−0.006	
N(n)	0.009 (5)[b]	0.001 (5)	−0.004 (5)	−0.001 (5)
C(n1)	−0.003 (6)	0.000 (6)	0.010 (6)	−0.001 (6)
C(n2)	−0.014 (6)	−0.001 (6)	0.015 (6)	0.003 (6)
C(n3)	−0.006 (6)	0.002 (6)	−0.007 (6)	−0.005 (6)
C(n4)	0.004 (6)	−0.002 (6)	−0.009 (6)	0.003 (6)
C(n5)	−0.004 (6)	0.001	−0.005 (6)	0.023
C(n6)	−0.010	0.008	−0.017	0.018
av dev	0.007	0.001	−0.004	0.003

	plane equation: $Ax + By + Cz = D$			
plane no.	A	B	C	D
1	0	0	6.720	2.516
2[c]	−0.096	−0.120	6.720	2.487
1′	0	0	6.720	0.891
2′[d]	0.108	−0.152	6.719	0.892

[a] Plane is defined by the porphyrin 24-atom core and corresponds to the z value indicated. [b] Standard deviations are given for those atoms used in the definition of the plane. [c] The dihedral angle between plane 1 and plane 2 is 0.53°. [d] The dihedral angle between plane 1′ and plane 2′ is 0.64°.

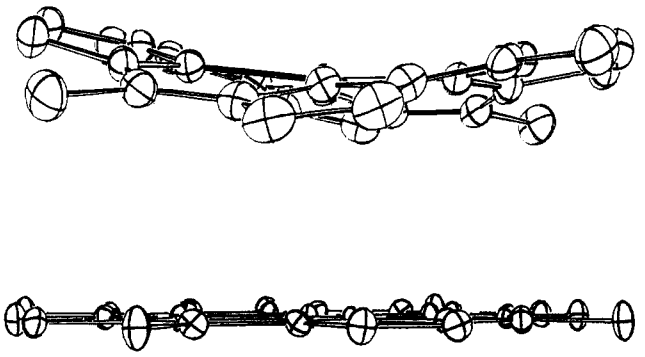

Figure 5. Comparison of the S_4-ruffled Ni(tmp) cation in $[Ni(tmp)]_2[PF_6]$ (top) and the planar Ni(tmp) cation in $[Ni(tmp)_2][ReO_4]$.

weighted least-squares planes are given in Table IV. This planarity, though similar to that found in the parent molecule,[19] is in marked contrast to previous tmp conductors where the cations exhibit S_4 ruffling and deviate by as much as 0.60 Å ($[Ni(tmp)]_2[PF_6]$)[11] and 0.55 Å (Ni(tmp)I)[1] from the best least-squares planes. Figure 5 contrasts this structural difference. The N–Ni–N angle for both Ni(tmp) cations of $[Ni(tmp)]_2[ReO_4]$ is by symmetry 90°, 0.17 (2)° less than that found in the nonplanar $[Ni(tmp)]_2[PF_6]$[11] structure. There is also a lengthening of the Ni–N bond distance in $[Ni(tmp)]_2[ReO_4]$. Thus, the Ni–N distances of 1.961 (4) and 1.956 (4) Å may be compared with that of 1.933 (2) Å in the PF_6 salt.

The ReO_4^- Anion. The ReO_4^- anion is ordered and is located on a site of imposed $\bar{4}$ symmetry (site 2b). As expected, the anion is essentially tetrahedral (∠O–Re–O = 109.3 (2)°). The Re–O distance of 1.729 (4) Å is normal.[20] We observed no peaks at the $^1/_4$, $^3/_4$, 0 position (site 2a) in a difference electron density map. The location of the ReO_4^- anion in site 2b as opposed to site 2a (also of $\bar{4}$ symmetry) may be rationalized in terms of anion-to-ring contacts. The two sites do not possess identical environments. Site 2a ($^1/_4$, $^3/_4$, 0) is more constrained than site 2b ($^1/_4$, $^3/_4$, $^1/_2$). The H···Re distances from the center of an ReO_4^- anion fixed at each site to the nearest ring atoms are ~3.0 Å for site 2a and ~3.5 Å for site 2b. Though on the less constrained site, the ReO_4^- anion is involved in three close H···O contacts:

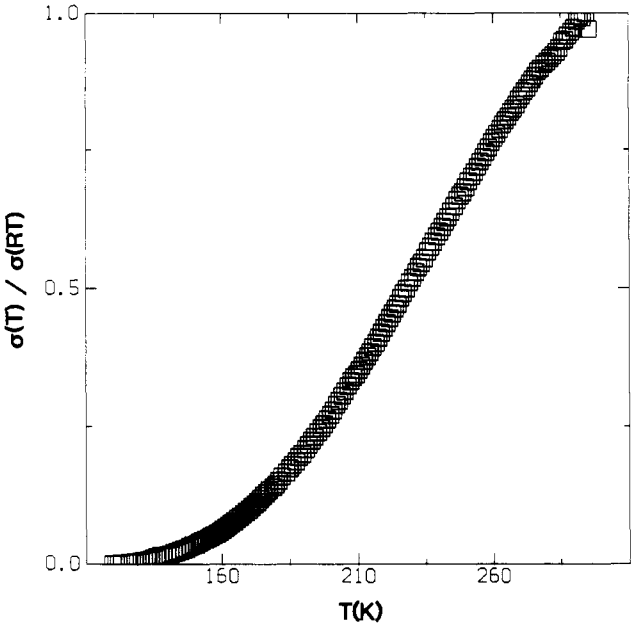

Figure 6. Temperature dependence of the conductivity for a single crystal of $[Ni(tmp)]_2[ReO_4]$. σ(298 K) = 95 Ω^{-1} cm^{-1}.

H(1)C(13)···O = 2.3 Å, H(1)C(16)···O = 3.0 Å, and H(2)C(16)···O = 3.1 Å. The expected van der Waals contact[13] is 2.6 Å.

Single-Crystal Electrical Conductivity. The room-temperature value of the electrical conductivity of $[Ni(tmp)]_2[ReO_4]$ single crystals measured along the needle (c) axis ranges from 75 to 115 Ω^{-1} cm^{-1}. These values are comparable to those observed for Ni(tmp)I[1] (40–270 Ω^{-1} cm^{-1}) and $[Ni(tmp)]_2[PF_6]$ (10–200 Ω^{-1} cm^{-1})[11] but are lower than those observed for the benzoporphyrin and phthalocyanine systems Ni(tbp)I[5] (150–330 Ω^{-1} cm^{-1}) and Ni(pc)I[6] (260–750 Ω^{-1} cm^{-1}).

In one-electron band theory the conductivity can be related to $\bar{\lambda}_\parallel$, the mean free path of a carrier along the stacking direction (the average distance between scattering events), and to A, the cross-sectional area per conducting stack, by the relation

$$\sigma_\parallel = 2e^2\bar{\lambda}_\parallel/(hA) \qquad (1)$$

where e is the electron charge and h is Planck's constant.[21] For $[Ni(tmp)]_2[ReO_4]$, $\bar{\lambda}_\parallel \sim 0.9$ Å, which is within the range found for Ni(tmp)I,[1] $\bar{\lambda}_\parallel \sim 0.5$ Å, and $[Ni(tmp)]_2[PF_6]$, $\bar{\lambda}_\parallel \sim 0.5$ Å.[11] When expressed in units of intermolecular spacing along the stacking direction $\bar{\lambda}_\parallel \sim {}^1/_4$. A value of $\bar{\lambda}_\parallel < 1$ in these units is generally associated with a diffusion or hopping conductor. For comparison, Ni(pc)I has $\bar{\lambda}_\parallel > 1$, an indication that the conduction process is significantly wavelike.[6]

The temperature dependence of the conductivity, normalized to the room-temperature value, is presented in Figure 6. This behavior can be fit precisely to a simple expression describing a semiconductor with a thermally activated carrier concentration and a temperature-dependent carrier mobility[22]

$$\sigma/\sigma_0 = T^{-\alpha}\exp(-E_g/kT) \qquad (2)$$

where σ/σ_0 is the normalized conductivity, α is a crystal-dependent mobility parameter, E_g is the band gap, and k is Boltzmann's constant. A least-squares fit of several data sets to eq 2 yields a band gap of E_g = 0.24 (2) eV and mobility parameters $\alpha \geq 3.5$. These high values of α demonstrate that the conductivity is strongly dependent on the mobility of the carriers.[22]

These results contrast with those of other Ni(tmp)-based conductors,[1,11] which display a metallic behavior upon cooling from

(19) Gallucci, J. C.; Swepston, P. N.; Ibers, J. A. *Acta Crystallogr.* **1982**, *B38*, 2134–2139.
(20) Hoffmann, R. *Angew. Chem., Int. Ed. Engl.* **1987**, *26*, 846–878.
(21) Berlinsky, A. *J. Contemp. Phys.* **1976**, *17*, 331–354.
(22) (a) Kittel, C. *Introduction to Solid State Physics*; Wiley: New York, 1976. (b) Epstein, A. J.; Conwell, E. M.; Sandman, D. J.; Miller, J. S. *Solid State Commun.* **1977**, *23*, 355–358.

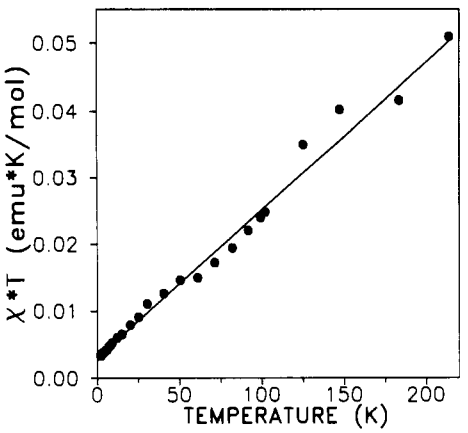

Figure 7. Temperature dependence of the product of temperature and paramagnetic susceptibility. The solid line is the theoretical fit.

room temperature and then reach a maximum conductivity at a temperature T_0, below which they become semiconducting (Ni(tmp)I, $T_0 \approx 110$ K;[1] [Ni(tmp)]$_2$[PF$_6$], $T_0 \approx 205$ K).[11] The conductivity of [Ni(tmp)]$_2$[ReO$_4$] from room temperature to 350 K shows no deviations from the behavior described by eq 2. Above 350 K the conductivity decreases irreversibly owing to sample decomposition.

Electron Spin Resonance Measurements. Powdered samples of [Ni(tmp)]$_2$[ReO$_4$] have a single, symmetric resonance with a g value near that of the free electron, $g = 2.004$ (1). Single-crystal measurements show that the g value of [Ni(tmp)]$_2$[ReO$_4$] is essentially isotropic, $g = 2.004$ (1), within the error of our measurements. The line width is narrow, 8.3 (4) G, and also is isotropic. The signal is weak, and spin susceptibility measurements indicate that it can be accounted for by 0.031 spins ($g = 2.004$) per macrocycle at room temperature. The spin susceptibility decreases as the temperature is lowered and is approximately 65% of its room-temperature value at 77 K. The low intensity of the ESR signal and the increase of the spin susceptibility with increasing temperature suggest that the carriers whose concentration also increases with T are responsible for at least a portion of the ESR signal. Bulk susceptibility data suggest that the carriers do not account for the total intensity of the ESR signal and that localized paramagnetic defect sites are also present in this material (vide infra). Therefore, the intensity of the ESR signal cannot be analyzed to give a direct measure of the carrier concentration.

Bulk Susceptibility Measurements. The measured room-temperature static susceptibility of a powdered sample of [Ni(tmp)]$_2$[ReO$_4$] is $\chi = -2.90 \times 10^{-4}$ emu/mol. When corrected for temperature-independent diamagnetism ($\chi^d = -5.39 \times 10^{-4}$ emu/mol),[23] the paramagnetic susceptibility is $\chi^p = 2.49 \times 10^{-4}$ emu/mol. This quantity is somewhat smaller than but comparable to the values measured for other Ni(tmp)-based conductors (Ni(tmp)I, $\chi^p = 3.63 \times 10^{-4}$ emu/mol;[1] [Ni(tmp)]$_2$[PF$_6$], $\chi^p = 3.72 \times 10^{-4}$ emu/mol).[11] The temperature dependences of the quantity $T\chi^p$ is shown in Figure 7. The data indicate that χ^p follows the expression

$$\chi^p = C/T + K \qquad (3)$$

where C is the Curie constant and K is a constant, temperature-independent contribution to the susceptibility; a fit of the data to the more general Curie–Weiss expression led to a value of zero for the Weiss constant. The first term in eq 3 represents a contribution to χ^p by noninteracting spins that have a temperature-dependent susceptibility that follows the Curie law. A least-squares fit of the data yields $C = 3.04$ (7) $\times 10^{-3}$ emu/mol K and $K = 2.21$ (4) $\times 10^{-4}$ emu/mol.

(23) From Pascals constants, see: (a) Drago, R. S. *Physical Methods in Chemistry*; W. B. Saunders: Philadelphia, PA, 1977; p 413. (b) Mulay, L. N.; Boudreaux, E. A., Eds. *Theory and Applications of Molecular Diamagnetism*; Wiley: New York, 1976; p 307.

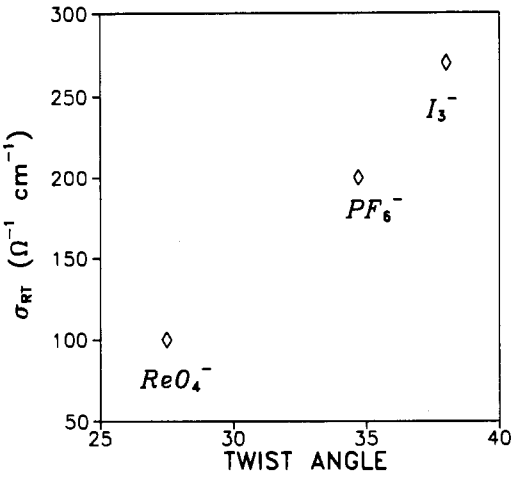

Figure 8. Best room-temperature conductivity plotted against the metallomacrocycle rotation angle, ϕ.

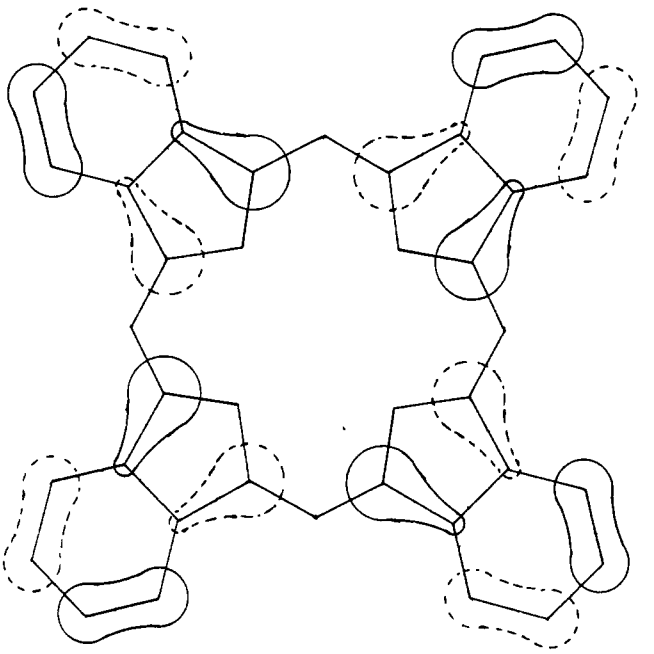

Figure 9. The a_{1u} molecular orbital of pc.

The magnitude of the Curie constant measured for [Ni(tmp)]$_2$[ReO$_4$] can be interpreted from the relation

$$C = S(S+1)\left(\frac{Ng^2\beta^2}{3k}\right) \qquad (4)$$

where β is the Bohr magneton, k is Boltzmann's constant, S is the spin, g is the Lande factor, and N is the number of localized noninteracting spin sites per mole. The measured Curie constant corresponds to $N = 8.3 \times 10^{-3}$ spins per Ni(tmp) molecule that are assigned to impurities or defect sites. Such Curie-like spins account for approxiimately 30% of the ESR signal intensity at room temperature; it is likely that the additional signal intensity is largely associated with the carriers. Because the carrier concentration is activated, as the temperature is lowered the contribution to the susceptibility of the carriers decreases exponentially but that of the localized spins increases in accordance with the Curie law so that at low temperatures the susceptibility is dominated by these localized spins.

The value of the temperature-independent paramagnetism, $K = 2.21 \times 10^{-4}$ emu/mol, is larger than would be expected for a simple semiconductor with a diamagnetic ground state. A large value of K also has been observed in the other Ni(tmp)-based conductors synthesized to date.[1,4,11] Because [Ni(tmp)]$_2$[ReO$_4$] is a semiconductor, its temperature-independent paramagnetism

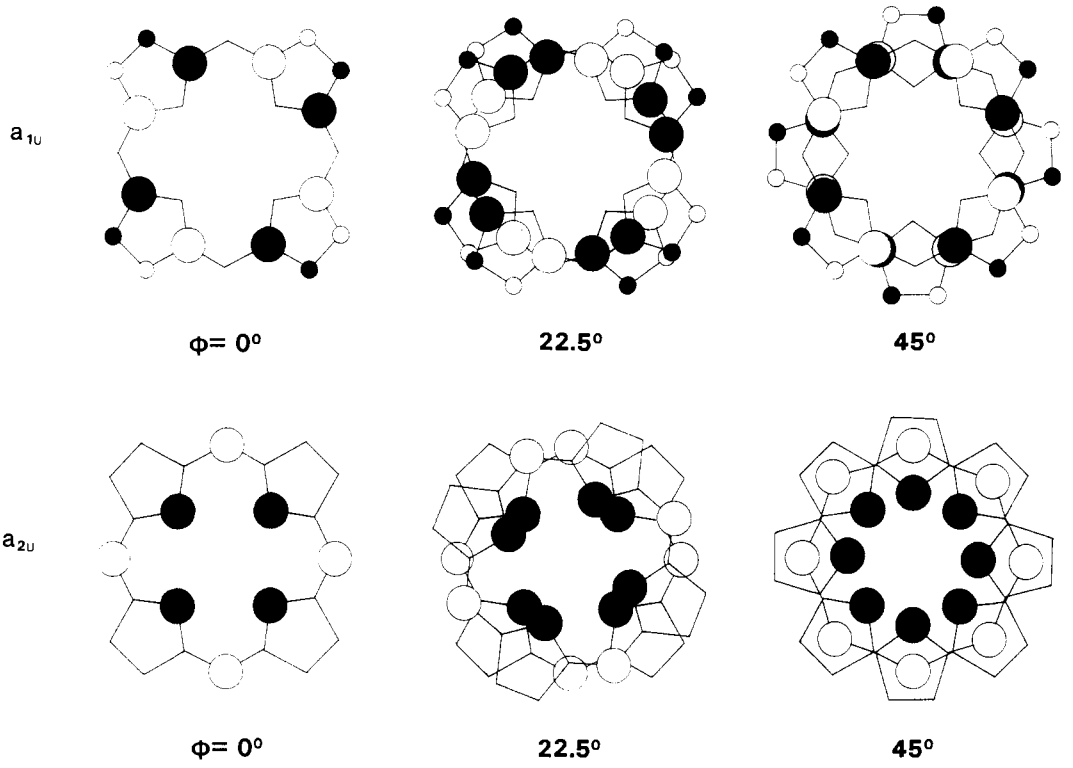

Figure 10. Overlap between a_{1u} and a_{2u} molecular orbitals at different rotation angles, ϕ.

cannot arise from Pauli paramagnetism of conduction electrons in a metallic band. Therefore, this contribution is most probably attributable to a Van Vleck paramagnetism that arises because the valence band or bands of the compounds are associated with the nearly degenerate a_{1u}, a_{2u} HOMO set of Ni(tmp).

Implications of the Structure. The Ni(tmp) cations are not constrained crystallographically to be equally spaced. Even so, the Ni(1)–Ni(2) distance of 3.355 (2) Å and the Ni(2)–Ni'(1) distance of 3.365 (2) Å are not significantly different. Even if there were a slight dimerization of the conducting stacks of the material, this could not be the reason that $[Ni(tmp)]_2[ReO_4]$ behaves in a semiconducting rather than a metallic fashion. Consider a conduction band formed from porphyrin π orbitals that contain two electrons per metallomacrocycle before partial oxidation of the macrocycle. To account for the 2:1 stoichiometry of $[Ni(tmp)]_2[ReO_4]$ one electron must be removed from every two Ni(tmp) molecules. This degree of partial oxidation then yields a $^3/_4$-filled π band. Dimerization of the conducting stacks would open a gap at the $^1/_2$-filled level of the π band, well below the Fermi level, and therefore would not render the material semiconducting. On the contrary, the intrastack ring separation is significantly shorter than that found in Ni(tmp)I[1] (3.44 Å) or $[Ni(tmp)]_2[PF_6]$[11] (3.50 Å) and is within the expected van der Waals contact (3.4 Å).[13] All factors being equal, such a small intermolecular spacing would increase the transfer integral between the π molecular orbitals of the porphyrins and would promote the formation of a wide band and metallic conductivity.

Instead, comparison with other macrocyclic conductors indicates that the semiconducting behavior of $[Ni(tmp)]_2[ReO_4]$ occurs because intrastack, intermolecular overlap is small at the 27.5° rotation angle (ϕ) between adjacent intrastack rings. Figure 8 shows that the room-temperature conductivities of Ni(tmp)-based conductors vary directly with ϕ. Furthermore, for Ni(tmp)I ϕ = 37 (1)° and the conductivity is metallic from room-temperature to 110 K, below which activated behavior is observed.[1] For $[Ni(tmp)]_2[PF_6]$ ϕ = 34.7 (2)° and a transition from metallic to activated behavior occurs at 205 K.[11] Finally, the large-ring benzoporphyrin-based conductors all possess rings rotated by ~40° and all are metallic down to low temperatures (except for Co(pc)I for reasons peculiar to that compound[3]). Theoretical investigations on $[Si(pc)O]_n$ systems in the context of a tight-binding band scheme[24] demonstrate a strong ϕ dependence of the bandwidth, and hence the conductivity. In these systems the conduction band arises from the overlap of the a_{1u} molecular orbital. The symmetry and location of this orbital are shown in Figure 9. Maximum overlap of this orbital between adjacent rings, and hence the maximum bandwidth and conductivity, occur when ϕ = 0 or 45°. At ϕ = 19° the bandwidth is predicted to be zero[24] and the conductivity is expected to be minimal.

Unlike those of benzoporphyrins such as phthalocyanine, the highest occupied molecular orbitals of simple porphyrins are the nearly degenerate a_{1u} and a_{2u} set. The transfer integral (overlap) between a_{2u} orbitals on adjacent rings is largest near ϕ = 0° and decreases as ϕ approaches 45° (Figure 9); the porphyrin a_{1u} molecular orbital behaves in an analogous way to the pc a_{1u} orbital (Figure 10). Thus, the gradual change from metallic to thermally activated behavior of 37, 34.7, and 27.5° for Ni(tmp)I,[1] $[Ni(tmp)]_2[PF_6]$,[11] and $[Ni(tmp)]_2[ReO_4]$, respectively, may reflect conductivity dominated by an a_{1u} band whose bandwidth is decreasing.

Acknowledgment. We thank Dr. Eric Liimatta for performing the EDAX experiments. We are grateful for the use of the SQUID susceptometer in the Chemistry Department and Center for Fundamental Materials Research at Michigan State University. We also thank Professor Mark Ratner for useful discussions. This work was supported by the National Science Foundation through Grant No. DMR-8818599 (B.M.H.) and through the Northwestern University Materials Research Center, Grant No. DMR-8821571.

Registry No. $[Ni(tmp)]_2[ReO_4]$, 124225-59-8; Ni(tmp), 67067-51-0; $[N(n\text{-}Bu)_4][ReO_4]$, 16385-59-4.

Supplementary Material Available: Complete crystallographic details (Table IS) and anisotropic thermal parameters (Table IIS) (3 pages); $10|F_o|$ vs $10|F_c|$ (Table IIIS) (12 pages). Ordering information is given on any current masthead page.

(24) Pietro, W. J.; Marks, T. J.; Ratner, M. A. *J. Am. Chem. Soc.* **1985**, *107*, 5387–5391.